Proceedings of the Canadian Society for Mechanical Engineering International Congress 2022
CSME Congress 2022
June 5-8, 2022, Edmonton, AB, Canada

Observer-based Super-twisting Sliding Mode Control of Quadcopters

Sean Smith, Ya-Jun Pan
Department of Mechanical Engineering
Dalhousie University, Halifax, Canada
s.smith@dal.ca, yajun.pan@dal.ca

Abstract—This paper focuses on the problematic position tracking of a quadcopter under external disturbances by developing a super-twisting sliding mode controller (STSMC) based on a higher-order sliding mode observer (HOSMO). A generalized quadcopter model is presented with position and attitude dynamics. This observer-based controller design is applied adaptable for future hardware implementation on a COEX Clover 4.2. The Clover drone has measurable position signal using vision-based navigation and ArUco marker localization, where the HOSMO can estimate the unknown state being linear velocity. HOSMO helps in estimating the unknown external disturbances on the quadcopter for possible compensations. The proposed controller has been applied to the position dynamics with extensive simulations. If desired, it could be applied to the attitude dynamics as well. Lyapunov-based method is used to investigate the closed-loop stability and convergence while a smoothing function was used to attenuate potential chattering problems.

Keywords – super-twisting sliding mode control; high-order observer; disturbances; quadcopter; nonlinearity

I. INTRODUCTION

The research and development of the Unmanned Aerial Vehicle (UAV) has grown extensively over the past few decades. Its application has expanded and is now implemented in a variety of sectors such as agriculture, transportation and delivery, mining, security, and filming to name a few. It is through these applications where their benefits came to light and UAVs became known to perform complex tasks such as military reconnaissance and surveillance, search and rescue, science data collection, and payload delivery while being able to operate in complex environments.

Throughout these applications the multirotor vehicle needs to perform maneuvers such as position tracking. Navigation through dangerous environments requires accurate position tracking of the vehicle and in a real-world setting system disturbance such as wind will be common. If the vehicle is not able to effectively perform and overcome these control problems, then damages may come about to the vehicle itself or even to the people involved.

This work was supported in part by the funding from the Innovation for Defense Excellence and Security (IDEaS) program the Department of National Defense (DND), Natural Sciences and Engineering Research Council (NSERC), and the Government of Nova Scotia, Canada.

Considerable research has been conducted around the control of multi-rotors particularly in reference tracking control. An overview of the main control strategies of both linear and nonlinear types can be found in [1]. Some of the main linear techniques include the Proportional Integral Derivative (PID) and Linear Quadratic Regulator (LQR) controllers. PID is the most common because of its simplicity and is easy to implement as it is not model based. This controller can be easily tuned to produce good results. The use of linear control methods has limitations where linearized dynamics restricts flight to a certain domain and a smaller flight envelop. This can be undesirable for many real-time applications.

To improve upon these limitations, nonlinear control strategies have been studied and implemented which have proven to expand control applications. Among the nonlinear controllers, feedback linearization is one of the more popular approaches [2, 3]. Backstepping is another nonlinear control technique developed to globally stabilize the overall system through a recursive control algorithm that works by designing intermediate control laws for some of the state variables [4].

Another nonlinear controller is the sliding mode controller (SMC) which is generally insensitive to unmodelled dynamics, parametric uncertainties and external disturbances. One major drawback with this control solution is the chattering phenomena that appears in the control law. To address this problem, the work in [5] presents the concept of high order sliding mode (HOSM), which can remove the requirement to have a relative degree of one as with conventional sliding mode and attenuate the effects of chattering phenomena [6]. This includes the twisting algorithm or super twisting sliding mode controller where the idea of acting on superior derivatives of the sliding variable was introduced.

To utilize such a control strategy, knowledge of all state variables would be required. When applying to hardware, there may not be sensors to measure the bounded disturbances, or all required states. Because of this, the introduction of observers has become a popular occurrence where they can be used to estimate unknown disturbances and states and offer more robustness by compensating uncertainties.

In [7], HOSMO was introduced with the super-twisting controller (STC) for a double integrator system to address the regulation problem despite the unmeasurable states and

unknown disturbances. The closed-loop asymptotic stability has been proven in [7]. This was extended in [8] where the observer-based controller was implemented on both position and attitude dynamics for finite-time trajectory tracking under external disturbances by using a non-linear sliding manifold to ensure the finite-time convergence of the tracking error.

Motivated by the literature work, this paper proposes to develop a super-twisting sliding mode controller based on a higher order sliding mode observer for reference tracking under external disturbances for Quadcopters. Simulation studies in Matlab/Simulink have been carried out to demonstrate the effectiveness of the approach. The purpose is to set up the observer-based control architecture for future implementation on hardware with the COEX Clover 4.2 drone available in the Advanced Control and Mechatronics (ACM) Lab at Dalhousie University. The Clover drone has a PX4 flight controller that implements a cascaded PID control structure with an inner loop for attitude control and an outer loop for position control. The design will be set up to replace the PID position control module. Using vision-based navigation with an ArUco marker map for position feedback, position can be determined, and velocity can be estimated with the observer.

II. Problem Formulation

A. Modelling

Consider the quadcopter (COEX Clover 4.2 drone) in Fig. 1, two coordinate frames are of interest. The first coordinate frame is the inertial frame $\mathbf{I} = \{\bar{x}_I, \bar{y}_I, \bar{z}_I\}$ described by the North East Down (NED) convention and the second is the body-fixed coordinate frame $\mathbf{B} = \{\bar{x}_B, \bar{y}_B, \bar{z}_B\}$.

A quadcopter can be modeled by a six degrees-of-freedom (DOFs) rigid body. The forces acting on this rigid body can be described by kinetic equations (1) and (2),

$$\mathbf{F_B} = m\dot{\mathbf{V}}_\mathbf{B} + \boldsymbol{\Omega}_\mathbf{B} \times (m\mathbf{V_B}), \tag{1}$$

$$\mathbf{M_B} = \mathbf{I}\dot{\boldsymbol{\Omega}}_\mathbf{B} + \boldsymbol{\Omega}_\mathbf{B} \times (\mathbf{I}\boldsymbol{\Omega}_\mathbf{B}), \tag{2}$$

where $\mathbf{F_B}$ and $\mathbf{M_B}$ are the body forces and moments acting on the quadcopter. Parameters m and $\mathbf{I}$ are the mass and moment of inertia of the quadcopter and $\boldsymbol{\Omega}_\mathbf{B}$ and $\mathbf{V_B}$ are the angular and linear velocities of the quadcopter in the body frame.

The model is derived using Euler angles and the kinematics can be represented by applying Newton's second law, where the position dynamics are seen in (3) and (4),

$$m\ddot{\boldsymbol{\eta}} = \mathbf{F}_\mathbf{I}^\mathrm{G} + \mathbf{R}\mathbf{F}_\mathbf{B}^\mathrm{T} + \boldsymbol{\xi}, \tag{3}$$

$$\begin{bmatrix} \ddot{x} \\ \ddot{y} \\ \ddot{z} \end{bmatrix} = \begin{bmatrix} 0 \\ 0 \\ g \end{bmatrix} + \begin{bmatrix} (C_\psi S_\theta C_\phi + S_\psi S_\phi) \\ (S_\psi S_\theta C_\phi - C_\psi S_\phi) \\ -(C_\theta C_\phi) \end{bmatrix} \left(\frac{U_z}{m}\right) + \begin{bmatrix} \xi_x \\ \xi_y \\ \xi_z \end{bmatrix}, \tag{4}$$

where $S_x = \sin(x)$, $C_x = \cos(x)$, $\boldsymbol{\eta} = [x\ y\ z]^T$ is the quadcopter's position in the inertial frame, $\mathbf{F}_\mathbf{I}^\mathrm{G} = [0\ 0\ g]^T$ is the gravitational force in the inertial frame, $\mathbf{F}_\mathbf{B}^\mathrm{T} = [0\ 0\ U_z]^T$ is the total thrust from the rotors in the body frame, $g = 9.81\ m/s^2$ is the gravitational constant, and $\boldsymbol{\xi} = \begin{bmatrix} \xi_x & \xi_y & \xi_z \end{bmatrix}^T$ is the unknown time-varying lumped external disturbances such as wind gusts on the system.

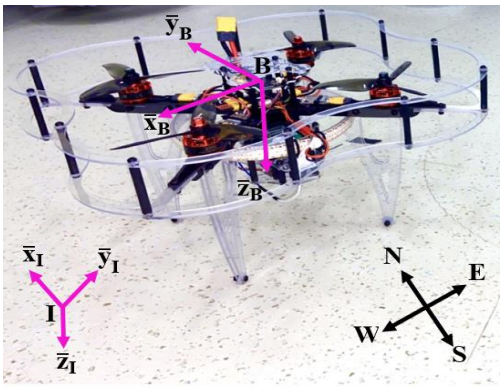

Figure 1. Quadcopter modelling coordinate frames (COEX Clover 4.2 drone at ACM-Lab, Dalhousie University)

The rotation matrix is defined as

$$R = \begin{bmatrix} C_\psi C_\theta & C_\psi S_\theta S_\phi - S_\psi C_\phi & C_\psi S_\theta C_\phi + S_\psi S_\phi \\ S_\psi C_\theta & S_\psi S_\theta S_\phi + C_\psi C_\phi & S_\psi S_\theta C_\phi - C_\psi S_\phi \\ -S_\theta & C_\theta S_\phi & C_\theta C_\phi \end{bmatrix},$$

which is an orthogonal rotation matrix that transforms from the body-fixed frame to the inertial frame.

Similarly, the attitude dynamics seen in (2) are in the body frame and after applying Newton's second law and considering the moments produced by the actuators and external disturbances, they can be represented with (5) and (6).

$$\mathbf{I}\dot{\boldsymbol{\Omega}}_\mathbf{B} = \boldsymbol{\Omega}_\mathbf{B} \times (\mathbf{I}\boldsymbol{\Omega}_\mathbf{B}) + \mathbf{M}_\mathbf{B}^\mathrm{T} + \mathbf{M}_\mathbf{B}^\mathrm{D}, \tag{5}$$

$$\begin{bmatrix} I_{xx}\dot{\Omega}_{B_x} \\ I_{yy}\dot{\Omega}_{B_y} \\ I_{zz}\dot{\Omega}_{B_z} \end{bmatrix} = \begin{bmatrix} (I_{yy} - I_{zz})\Omega_{B_y}\Omega_{B_z} \\ (I_{zz} - I_{xx})\Omega_{B_x}\Omega_{B_z} \\ (I_{xx} - I_{yy})\Omega_{B_x}\Omega_{B_y} \end{bmatrix} + \begin{bmatrix} U_\phi \\ U_\theta \\ U_\psi \end{bmatrix} + \begin{bmatrix} M_\phi \\ M_\theta \\ M_\psi \end{bmatrix}, \tag{6}$$

where $\mathbf{M}_\mathbf{B}^\mathrm{T} = \begin{bmatrix} U_\phi & U_\theta & U_\psi \end{bmatrix}^T$ are the input moments on the quadcopter and $\mathbf{M}_\mathbf{B}^\mathrm{D} = \begin{bmatrix} M_\phi & M_\theta & M_\psi \end{bmatrix}^T$ are the moments produced by the time-varying lumped disturbances such as wind gusts. In this paper the aerodynamic and gyroscopic effects are not considered in the modeling.

B. General Second-Order System

This section presents a general second-order system which the observer-based controller will be developed on before applying it to the quadcopter dynamics to solve the reference tracking control problem. This second-order system can be represented by the following model

$$\begin{cases} \dot{x}_1 = x_2, \\ \dot{x}_2 = f(x) + h(x)u + \xi(x), \\ y = x_1, \end{cases} \tag{7}$$

where $x(t) = [x_1\ \ x_2]^T \in \mathbb{R}^2$ is the system state vector, $f(x) \in \mathbb{R}$ and $h(x) \in \mathbb{R}$ are known functions and $y = x_1$ is the measurable system output. Lastly, $\xi(t)$ is the unknown time-varying lumped disturbance on the system dynamics with ξ_s being its upper bound where $|\xi(t)| \leq \xi_s$.

III. Higher-order Sliding Mode Observer Design

The HOSMO is designed to estimate the dynamics x_2 along with the system disturbance ξ in (7) as

$$\begin{cases} \dot{\hat{x}}_1 = \hat{x}_2 + \lambda_1 |\tilde{x}_1|^{\frac{2}{3}} \text{sign}(\tilde{x}_1), \\ \dot{\hat{x}}_2 = \hat{x}_3 + \lambda_2 |\tilde{x}_1|^{\frac{1}{3}} \text{sign}(\tilde{x}_1) + f(x) + h(x)u, \\ \dot{\hat{x}}_3 = \lambda_3 \text{sign}(\tilde{x}_1), \end{cases} \tag{8}$$

where $\dot{\hat{x}}_i$, $i = 1,2,3$, represents the estimated values of the states. The estimation errors are defined as $\tilde{x}_1 = x_1 - \hat{x}_1$ where $\tilde{x}_2$ and $\tilde{x}_3$ are defined analogously. Let $x_3 = \xi$, and the initial value of $\hat{x}_3$ is assumed to be zero for simplicity. Considering a new estimation error variable $\tilde{x}_3 = \xi - \hat{x}_3$, then from (7) and (8), the estimation error dynamics can be written as

$$\begin{cases} \dot{\tilde{x}}_1 = \tilde{x}_2 - \lambda_1 |\tilde{x}_1|^{\frac{2}{3}} \text{sign}(\tilde{x}_1), \\ \dot{\tilde{x}}_2 = \tilde{x}_3 - \lambda_2 |\tilde{x}_1|^{\frac{1}{3}} \text{sign}(\tilde{x}_1), \\ \dot{\tilde{x}}_3 = \dot{\xi} - \lambda_3 \text{sign}(\tilde{x}_1). \end{cases} \tag{9}$$

The above equation has the form of a non-recursive exact robust differentiator [8]. Therefore, (9) is finite-time stable and it has been proven in [9] using geometric methods and in [10] using a quadratic and strict Lyapunov function. We can conclude that the errors, $\tilde{x}_1$, $\tilde{x}_2$, and $\tilde{x}_3$ will converge to zero in a finite time $t > t_0$ if the gains λ_1, λ_2, and λ_3 are chosen appropriately [11]. After the convergence of the estimation error, it can be derived that $x_1 = \hat{x}_1$, $x_2 = \hat{x}_2$, and $x_3 = \hat{x}_3$ after finite time $t > t_0$.

IV. Super-Twisting Sliding Mode Controller Design

The goal is to design a super-twisting sliding mode controller based on the estimated state information for system (7) to track a reference trajectory in a finite time with the presence of external disturbances and modelling uncertainties. For this system, the position component x_1 is measurable and available while the velocity x_2 will be estimated with the observer $\hat{x}_2$. For second-order sliding mode control, the following convergence condition should be verified $s(x) = \dot{s}(x) = 0$ where $s(x)$ represents the sliding manifold of the following form

$$s = c_1 e_1 + \hat{e}_2 = 0, \tag{10}$$

where $c_1 > 0$, $e_1 = x_1 - x_1^d$, and $\hat{e}_2 = \hat{x}_2 - \dot{x}_1^d$. The desired position and velocity are denoted as x_1^d and $x_2^d = \dot{x}_1^d$ respectively. Taking the derivative of the sliding manifold (10) and substituting the system and observer dynamics gives

$$\begin{aligned} \dot{s} = c_1 \hat{x}_2 - c_1 \dot{x}_1^d + \int_0^t \lambda_3 \text{sign}(\tilde{x}_1) dt + \\ \lambda_2 |\tilde{x}_1|^{\frac{1}{3}} \text{sign}(\tilde{x}_1) + f(x) + h(x)u - \dot{x}_2^d. \end{aligned} \tag{11}$$

The control input is chosen such that the second order sliding mode occurs in finite time. This is given as,

$$\begin{aligned} u = h(x)^{-1}[- c_1 \hat{x}_2 + c_1 \dot{x}_1^d - \int_0^t \lambda_3 \text{sign}(\tilde{x}_1) dt - \\ \lambda_2 |\tilde{x}_1|^{\frac{1}{3}} \text{sign}(\tilde{x}_1) - f(x) + \dot{x}_2^d - k_1 |s|^{\frac{1}{2}} \text{sign}(s) - \\ \int_0^t k_2 \text{sign}(s) dt]. \end{aligned} \tag{12}$$

The control law (12) consists of two parts, one being the equivalent control and the other being the switching control. The equivalent control is responsible for maintaining the motion on the sliding surface and the switching control is responsible for forcing the trajectory towards the sliding surface despite the bounded uncertainties and external disturbances [8].

Substitution of the super-twisting control law (12) into (11) gives the following reaching law,

$$\dot{s} = - k_1 |s|^{\frac{1}{2}} \text{sign}(s) - \int_0^t k_2 \text{sign}(s) dt. \tag{13}$$

Defining $\eta = - \int_0^t k_2 \text{sign}(s) dt$, we have

$$\begin{cases} \dot{s} = - k_1 |s|^{\frac{1}{2}} \text{sign}(s) + \eta, \text{ and} \\ \dot{\eta} = - k_2 \text{sign}(s). \end{cases} \tag{14}$$

From (7) and (8), the sliding manifold in (10) can be rewritten as

$$s = x_2 - \tilde{x}_2 - \dot{x}_1^d + c_1 e_1, \tag{15}$$

and knowing $\dot{x}_1 \rightarrow x_2$ after some finite time t_0, one can write

$$\dot{x}_1 = s + \tilde{x}_2 + \dot{x}_1^d - c_1 e_1. \tag{16}$$

V. Stability Analysis

The closed-loop dynamics with the STSMC and HOSMO can be summarized as

$$\begin{aligned} \text{Y:} & \begin{cases} \dot{x}_1 = s + \tilde{x}_2 + \dot{x}_1^d - c_1 (x_1 - x_1^d), \\ \dot{s} = - k_1 |s|^{\frac{1}{2}} \text{sign}(s) + \eta, \\ \dot{\eta} = - k_2 \text{sign}(s), \end{cases} \\ \Pi\text{:} & \begin{cases} \dot{\tilde{x}}_1 = \tilde{x}_2 - \lambda_1 |\tilde{x}_1|^{\frac{2}{3}} \text{sign}(\tilde{x}_1), \\ \dot{\tilde{x}}_2 = \tilde{x}_3 - \lambda_2 |\tilde{x}_1|^{\frac{1}{3}} \text{sign}(\tilde{x}_1), \text{ and} \\ \dot{\tilde{x}}_3 = \dot{\xi} - \lambda_3 \text{sign}(\tilde{x}_1). \end{cases} \end{aligned} \tag{17}$$

A. Analysis of Subsystem Π

It was discussed earlier in section III that the estimation error of system Π converges to zero in finite time [12, Theorem 5.1]. Therefore, one can substitute $\tilde{x}_1 = \tilde{x}_2 = 0$ into (17).

The estimation error convergence is further proven by [8] where the authors in [10] have proposed a Lyapunov function for $|\dot{\xi}| \leq \xi_s$ as

$$V_1 = \vartheta^T \Gamma \vartheta, \tag{18}$$

where $\vartheta = \begin{bmatrix} |\tilde{x}_1|^{\frac{2}{3}} \text{sign}(\tilde{x}_1) & \tilde{x}_2 & |\tilde{x}_3|^2 \text{sign}(\tilde{x}_3) \end{bmatrix}^T$ and

$$\Gamma=\begin{bmatrix} \gamma_1 & \frac{1}{2}\gamma_{12} & 0 \\ -\frac{1}{2}\gamma_{12} & \gamma_2 & -\frac{1}{2}\gamma_{23} \\ 0 & -\frac{1}{2}\gamma_{23} & \gamma_3 \end{bmatrix}.$$

This implies that V_1 is positive definite and radially unbounded if and only if $\Gamma > 0$. The following conditions must be satisfied to ensure $\Gamma > 0$ [10, Theorem 1]

$$\gamma_1 > 0, \quad \gamma_1\gamma_2 > \frac{1}{4}\gamma_{12}^2,$$
$$\gamma_1\left(\gamma_2\gamma_3 - \frac{1}{4}\gamma_{23}^2\right) > \frac{1}{4}\gamma_1^2\gamma_3,$$

and in this case V_1 satisfies the differential inequality

$$\dot{V}_1 \leq -\kappa V_1^{\frac{3}{4}}, \tag{19}$$

for some positive κ therefore it is clear the estimation error will converge to zero in finite time for every value of derivative perturbation $|\dot{\xi}| \leq \xi_s$.

B. Analysis of Subsystem Υ

When the estimation error becomes zero, the closed loop system becomes

$$\begin{cases} \dot{x}_1 = s + \dot{x}_1^d - c_1(x_1 - x_1^d), \\ \dot{s} = -k_1|s|^{\frac{1}{2}}\text{sign}(s) + \eta, \\ \dot{\eta} = -k_2\text{sign}(s). \end{cases} \tag{20}$$

As stated in [7], the lower two equations in (20) are a super-twisting algorithm (STA), therefore by selecting appropriate gains $k_1 > 0$ and $k_2 > 0$ then $\dot{s} = s = 0$ in finite time.

This is further proven in [8] by choosing a candidate Lyapunov function as [13],

$$V_2 = \zeta^T P \zeta, \tag{21}$$

where $\zeta = \begin{bmatrix} |s|^{\frac{1}{2}}\text{sign}(s) & \eta \end{bmatrix}^T$ and the derivative vector is given by

$$\dot{\zeta} = \frac{1}{|\zeta_1|}A\zeta, \quad A = \begin{bmatrix} -\frac{k_1}{2} & \frac{1}{2} \\ -k_2 & 0 \end{bmatrix},$$

where $|\zeta_1| = |s|^{\frac{1}{2}}$, and taking the time derivative of (21) gives

$$\dot{V}_2 = \dot{\zeta}^T P\zeta + \zeta^T P\dot{\zeta},$$
$$= -|s|^{-\frac{1}{2}}\zeta^T Q\zeta,$$

where P and Q are related by the Algebraic Lyapunov Equation (ALE) $A^TP + PA = -Q$. Noting that A is Hurwitz if $k_1 > 0$ and $k_2 > 0$, it has been proven in [13, Theorem 1] that the stability of the equilibrium $s = 0$ is completely determined by the stability of matrix A. Therefore, the second-order sliding mode phenomena will occur and s and $\dot{s}$ will converge to zero in finite time.

Once $s = 0$, the closed loop dynamics will reduce to (22) and the asymptotic convergence of tracking error e_1 can be attained.

$$\dot{e}_1 = -c_1e_1, \tag{22}$$

considering another Lyapunov function as

$$V_3 = \tfrac{1}{2}e_1^2, \tag{23}$$

and taking the time derivative of (23) gives

$$\dot{V}_3 = e_1\dot{e}_1 = e_1(-c_1e_1) = -c_1e_1^2.$$

Therefore, e_1 is asymptotically stable by suitably selecting $c_1 > 0$ where $\dot{V}_3 < 0$. This further ensures the convergence of x_1 to x_1^d.

VI. Position Control of Quadcopter

A. Application to the Position Control Module

The Quadcopters translation dynamics presented in (4) can be represented with the following equations

$$\begin{aligned} \dot{x} &= v_x, \\ \dot{v}_x &= u_x + \xi_x, \\ \dot{y} &= v_y, \\ \dot{v}_y &= u_y + \xi_y, \\ \dot{z} &= v_z, \\ \dot{v}_z &= u_z + \xi_z, \end{aligned} \tag{24}$$

where u_x, u_y, and u_z are defined as virtual control inputs and are defined as

$$\begin{cases} u_x = \left(C_\psi S_\theta C_\phi + S_\psi S_\phi\right)\left(\frac{U_z}{m}\right), \\ u_y = \left(S_\psi S_\theta C_\phi - C_\psi S_\phi\right)\left(\frac{U_z}{m}\right), \\ u_z = g - \left(C_\theta C_\phi\right)\left(\frac{U_z}{m}\right). \end{cases} \tag{25}$$

To track a desired trajectory x^d, y^d, and z^d, we will utilize the super-twisting controller based on the higher order sliding mode observer developed in Sections III and IV. The observer (8) applied to the x-dynamics is shown:

$$\begin{cases} \dot{\hat{x}} = \hat{v}_x + \lambda_{x1}|\tilde{x}|^{\frac{2}{3}}\text{sign}(\tilde{x}), \\ \dot{\hat{v}}_x = \hat{\xi}_x + \lambda_{x2}|\tilde{x}|^{\frac{1}{3}}\text{sign}(\tilde{x}) + u_x, \\ \dot{\hat{\xi}}_x = \lambda_{x3}\text{sign}(\tilde{x}), \end{cases} \tag{26}$$

and the representation would be the same for the y and z dynamics. Now we can design the STSMC based on the estimated state information. For that, consider the sliding surface for the x-dynamics

$$s_x = c_{1x}\left(x - x^d\right) + \hat{v}_x - v_x^d, \tag{27}$$

where $c_{1x} > 0, \in \mathbb{R}^+$. The virtual controller for (24) is

$$\begin{aligned} u_x = &-c_{1x}\hat{v}_x + c_{1x}\dot{x}^d - \int_0^t \lambda_{3x}\text{sign}(\tilde{x})dt - \\ &\lambda_{2x}|\tilde{x}|^{\frac{1}{3}}\text{sign}(\tilde{x}) + \dot{v}_x^d - k_{1x}|s_x|^{\frac{1}{2}}\text{sign}(s_x) - \\ &\int_0^t k_{2x}\text{sign}(s_x)dt, \end{aligned} \tag{28}$$

and the virtual controller above guarantees that x tracks asymptotically to x^d. The virtual control definitions (25) can be rearranged into the following nonlinear decoupling equations [14]

$$U_z = m\sqrt{u_x^2 + u_y^2 + (u_z - g)^2},$$
$$\phi^d = \arcsin\left(\frac{m}{U_z}\left(u_x \sin\psi^d - u_y \cos\psi^d\right)\right), \quad (29)$$
$$\theta^d = \arctan\left(\frac{1}{u_z - g}\left(u_x \cos\phi^d + u_y \sin\phi^d\right)\right),$$

where this correction block determines the necessary angles ϕ^d, θ^d and the desired total thrust U_z. In this work, it is assumed the onboard attitude controller in the PX4 can track the desired roll and pitch angles provided by the position control module as described: $\phi(t) \rightarrow \phi^d(t)$ and $\theta(t) \rightarrow \theta^d(t)$ as $t \rightarrow \infty$.

B. Chattering Analysis

One feature of SMCs is the discontinuous switching component sign(s) that is used to maintain the trajectories on the surface $s = 0$. In order to deal with the unmodelled dynamics and disturbances, s is typically always varying about zero, causing the control to switch signs in order to maintain $s = 0$. This creates an undesirable effect known as chattering. An analysis on chattering was completed in [8] and it was determined that the chattering phenomenon was greatly increased due to the unmodelled dynamics. Moreover, increasing the value of the gain λ_3 to overcome the effect of growing disturbance will lead to increased chattering amplitude. It was concluded that chattering is present for the super-twisting algorithm but can be alleviated by properly selecting the gain parameters. It should be noted that the value of the gains is limited because the effect of disturbance is getting canceled by the disturbance estimation from the HOSMO resulting in reduced chattering.

Another method to smooth the chattering is replacing the sign(s) with a smooth function such as a saturation $\text{sat}(s/\epsilon)$ where ϵ is a small constant. This places a margin around $s = 0$ so that the sensitivity is reduced and when the trajectories are within the margins around $s = 0$, then the control is successful. The demonstrated results are as in Section VII.

VII. Simulation Results

In this section, the proposed observer-based controller is applied to the quadcopter dynamics to solve the reference tracking control problem with simulations. The virtual controllers developed for the STSMC-HOSMO pair on the dynamics (24) are simulated while under time-varying disturbances. The STSMC-HOSMO pair is applied on the position dynamics only, therefore observing the decoupling equations (29), the required physical characteristic needed is the mass of the quadcopter. The decoupling equations and mass would be used when implemented in the hardware within the on-board control system. Therefore, the mass of the COEX Clover would need to be identified.

For the first position tracking simulation using the STSMC-HOSMO, the translational system represented by (24) was made to track a circular

$$x^d = a\cos(t),$$
$$y^d = a\sin(t), \quad (30)$$
$$z^d = bt.$$

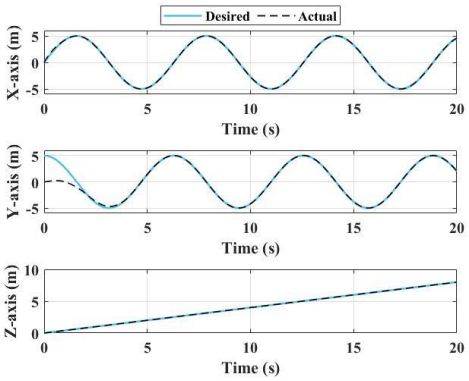

Figure 2. Translational response under the proposed controller for a quadcopter

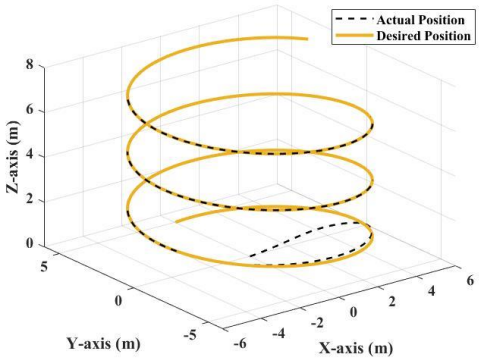

Figure 3. Tracking response under the proposed controller in a 3D space

The helix has a radius of "a", a slope of b/a, and t represents the time variation and when increased the desired trajectory (x^d, y^d, z^d) traces a right-handed helix with a pitch of $2\pi b$ about the z-axis. In this scenario, both the HOSMO and initial states' values are set to zero. The lumped external disturbances are chosen as $\xi_x = 0.6\sin(t)$, $\xi_y = 0.4\sin(t)$, and $\xi_z = 0.2\sin(t)$.

For this simulation, the radius was selected as $a = 5$ m and parameter b was set to 0.4 m giving a slope of $a/b = 12.5$ for the helix. Upon sufficient gain tuning, it is clear that the controller design is successful in position tracking under the influence of external disturbances where the translational dynamic tracking can be seen in Fig. 2. The actual (x, y, z) is the quadcopters position (dashed line) while the desired (x, y, z) are the desired reference trajectories (solid line). The x and y positions begin on the desired ones and maintain the position without any noticeable deviation even under the influence of external disturbances.

Considering the well performing position tracking, it is convenient to view the three-dimensional tracking of the circular helix which is shown in Fig. 3. While the dynamics were tracking the desired reference trajectory, the controller was also rejecting the time-varying external disturbances based on the estimations from the HOSMO. An illustration of the system disturbances along with their estimations from the HOSMO can be seen in Fig. 4.

What stands out in both the disturbance estimation and the

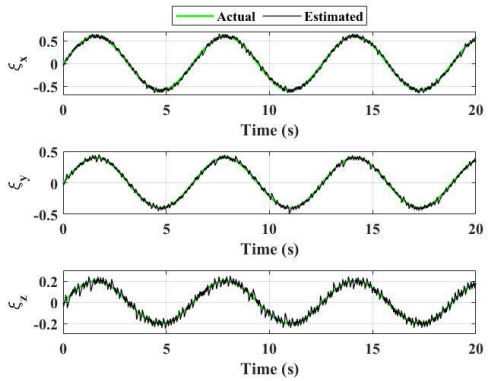

Figure 4. Profiles of the time-varying external system disturbance and the estimated system disturbance via a HOSMO observer

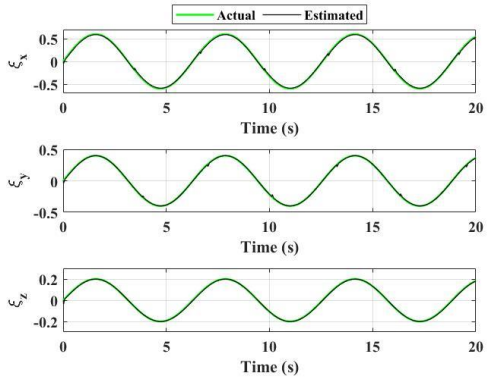

Figure 5. Profiles of the time-varying external system disturbance and the estimated system disturbance via observer with a smoothing function

control input is the chattering effect which was discussed at the end of Section VI.B. This effect has been increased due to the unmodelled dynamics; however, this is expected in the presence of external disturbances. This can have consequences on the continuity of the control input. The method proposed in Section VI.B to alleviate this chattering in the control input was by replacing the function sign(s) with a saturation function $\text{sat}(s/\epsilon)$ for the disturbance estimation in the HOSMO which is fed to the virtual control input for disturbance rejection. The constant was selected as a small constant $\epsilon = 0.000001$. The resulting disturbance rejection and virtual control input after this application can be seen in Fig. 5. The reduced chattering is noticeable where the smoothing function worked very well. Although the precision is reduced by this, the impact on the position tracking was negligible. During simulation, the disturbance rejection response and virtual control input response are much improved.

VIII. CONCLUSIONS

This paper addressed a control problem of the position tracking that is basic in nature but very important in research with its application common in quadcopter applications. For the position tracking problem, a STSMC based on a HOSMO observer was presented. This control strategy was implemented on the position dynamics and by defining virtual controllers, the proposed controller could be designed based on simplified dynamics and was designed as an improvement upon the standard SMC as it attenuates the chattering affect. Furthermore, the HOSMO provides an estimation of the velocity as well as the external disturbance introduced to the system. From the results and analysis, it was determined that the external disturbance is estimated and rejected very well and tracking the circular helix was successful.

To alleviate the chattering problem, a smoothing scheme was used in the disturbance estimation of the HOSMO that is fed to the control input for rejection. From this, the results were satisfactory as the chattering was alleviated and the influence on the position tracking was negligible. This removes any concern when applying to hardware in the future.

Future work will involve replacing the position control module in the PX4 control structure with this designed controller on the COEX Clover 4.2 drone in ACM-Lab at Dalhousie University. That was the motivation in designing a controller based on the position dynamics alone. Experiments will then be run using the Clover and ArUco marker localization with vision-based position feedback via the onboard camera to replicate the simulations.

REFERENCES

[1] S.Kumar and L. Dewan, "Different control scheme for the quadcopter: A brief tour," in *2020 First IEEE International Conference on Measurement, Instrumentation, Control and Automation (ICMICA)*, pp. 1-6, 2020.

[2] T. Tengis and A. Batmunkh, "State feedback control simulation of quadcopter model," in *2016 11th International Forum on Strategic Technology (IFOST)*, pp. 553-557, 2016.

[3] F. Sabatino, "Quadrotor control: modeling, nonlinearcontrol design, and simulation," 2015.

[4] V. K. Tripathi, L. Behera, and N. Verma, "Design of sliding mode and backstepping controllers for a quadcopter," in *2015 39th National Systems Conference (NSC)*, pp. 1-6, 2015.

[5] A. Levant, "Sliding order and sliding accuracy in sliding mode control," *International journal of control*, vol. 58, no. 6, pp. 1247-1263, 1993.

[6] V. Utkin, "Discussion aspects of high-order sliding mode control," *IEEE Transactions on Automatic Control*, vol. 61, no. 3, pp. 829-833, 2015.

[7] A. Chalanga, S. Kamal, L. M. Fridman, B. Bandyopadhyay, and J. A. Moreno, "Implementation of super-twisting control: Super-twisting and higher order sliding-mode observer-based approaches," *IEEE Tranactions on Industrial Electronics*, vol. 63, no. 6, pp. 3677-3685, 2016.

[8] V. K. Tripathi, A. K. Kamath, L. Behera, N. K. Verma, and S. Nahavandi, "Finite-time super twisting sliding mode controller based on higher-order sliding mode observer for real-time trajectory tracking of a quadcopter," *IET Control Theory & Applications*, vol. 14, no. 16, pp. 2359-2371, 2020.

[9] M. T. Angulo, J. A. Moreno, and L. Fridman, "Robust exact uniformly convergent arbitary order differentiator," *Automatica*, vol. 49, no. 8, pp. 2489-2495, 2013.

[10] J. A.Moreno, "Lyapunov function for levant's second order differentiator," in *2012 IEEE Conference on Decision and Control (CDC)*, pp. 6448-6453, 2012.

[11] A. Levant, "Homogeneity approach to high-order sliding mode design," *Automatica*, vol. 41, no. 5, pp. 823-830, 2005.

[12] J. A. Moreno, "Alyapunov approach to output feedback control using second-order sliding modes," *IMA Journal of Mathematical Control and Information*, vol. 29, no. 3, pp. 291-308, 2012.

[13] J. A. Moreno and M. Osorio, "Strict lyapunov functions for the super-twisting algorithm," *IEEE Transactions on Automatic Control*, vol. 57, no. 4, pp. 1035-1040, 2012.

[14] E. Paiva, H. Fretes, J. Rodas, M. Saad, Y. Kali, J. Lesme, and F. Lesme, "A comparative study of sliding-mode-based control strategies of a quad-rotor uav," in *IECON 2021 47th Annual Conference of the IEEE Industrial Electronics Society*, pp. 1-6, 2021.